MDPI

Article

Multi-Objective Optimization of Graded Thermal Storage System for Direct Steam Generation with Dish Concentrators

Zhengyue Zhu, Ruihao Bian, Yajun Deng *, Bo Yu and Dongliang Sun

School of Mechanical Engineering, Beijing Institute of Petrochemical Technology, Beijing 102617, China
* Correspondence: dengyajun@bipt.edu.cn

Abstract: A single sensible thermal storage system has the disadvantage of poor system efficiency, and a sensible-latent graded thermal storage system can effectively solve this problem. Moreover, the graded thermal storage system has the virtue of being adjustable, which can be adapted to many power generation systems. Therefore, this paper first analyzes the influence factors of the graded thermal storage system's exergy and thermal efficiency. Subsequently, each factor's significance was analyzed using the response surface method, and the prediction model for system exergy efficiency and cost was established using the support vector machine method. Finally, the second-generation nondominated sorting genetic algorithm (NSGA-II) was used to globally optimize the graded thermal storage system's exergy efficiency and cost by Matlab software. As a result, the exergy efficiency was increased by 11.01%, and the cost was reduced by RMB 5.85 million. In general, the effect of multi-objective optimization is obvious.

Keywords: sensible-latent graded thermal storage system; dish type solar thermal power; direct steam generation; multi-objective optimization

1. Introduction

Concentrated solar power with thermal energy storage (TES) is an essential solar thermal power (STP) technology. When the sunlight is insufficient or the power grid needs peak shaving, the stored thermal energy is converted to electric energy to meet the demand for a stable power supply [1–3]. Therefore, STP is a promising generation technology for renewable energy. Sunlight is concentrated on the heat absorber through the parabolic reflector, and the working medium is heated. Then, the high pressure and temperature steam is generated to drive the turbine to achieve electric energy. STP technology can be divided into four types: tower, dish, trough, and linear Fresnel [4–6]. Compared with the other three forms, the dish-type STP has a simple structure, flexible layout, higher power generation efficiency, and great potential for cost reduction [7]. In addition, different positions and different energies of solar energy have minimal impact on the dish-type STP. Currently, research on the dish-type STP is mainly focused on solar Stirling power generation. However, this type of power generation system cannot store heat and does not have the capability of stable and continuous power output, so it cannot be applied to commercial applications. Therefore, research on dish-type STP with TES is urgently needed.

According to the heat storage principle, TES technologies include thermochemical heat storage and thermophysical heat storage (sensible and latent TES) [8]. The thermochemical TES has a much higher energy density than the thermophysical TES. Sensible TES has the advantages of low cost, simple principles, convenient management, etc., and is widely used in the STP field. The benefits of latent TES are high TES density, relatively small heat storage volume, and slight temperature fluctuation [9–11]. In the dish-type STP, water as the heat transfer medium has the characteristics of no pollution, no corrosion, and low price. At the same time, direct steam generation technology is mature and has good application prospects [12–14]. However, the water-working medium undergoes a phase

change, and it is difficult for a single sensible TES to match the temperature–enthalpy curve of the water-working medium, resulting in a large energy loss. The graded TES, which couples sensible and latent TES, can solve this problem. The graded TES has a broader range of adjustable parameters and can be adapted to various power generation systems compared with the single-stage TES. However, minimal research on graded TES restricts its development and application to some degree.

Among the graded TES, the sensible-latent graded TES is mostly studied. In 2009, Laing et al. [15] first proposed a solid concrete three-tank graded sensible-latent graded TES. The material's melting point shows that the phase change material (PCM) uses sodium nitrate ($NaNO_3$). To study the process of heat storage/release for the graded TES, the German Aerospace Center [16] has built a sensible-latent graded TES for the Spanish direct steam power generation system. To improve the PCM's thermal conductivity, Laing et al. [15] used a PCM system containing aluminum fins and tested this system for 172 cycles at 400 °C/11.0 MPa. The results showed that the PCM would not degrade and had a reasonable heat storage/heat release rate. This experimental system's successful implementation guaranteed the later experiments' safety. Additionally, it confirmed the feasibility of applying sensible-latent graded TES in direct steam solar thermal power generation.

Birnbaum et al. [17] studied the direct steam generation power system based on Spain's 50 MW installed capacity power station. It was found that the temperature of the reheated steam was significantly lower than that of the main steam. Guo et al. [18] proposed a three-tank graded TES, in which a sensible TES consists of two-tank indirect TES and two heat exchangers. An intermediate buffer tank is added, and the mass flow rate of liquid sensible heat storage material could be adjusted according to the temperature–enthalpy characteristic curve of hydraulic characteristics so that the temperature–enthalpy characteristic curve of heat storage material could be better matched with water-based working medium and the system efficiency is improved. Guo et al. [19] compared the exergy efficiency and thermal efficiency of the two-tank sensible, three-tank sensible, and two-tank sensible-latent graded TES based on the previous three-stage graded TES through thermodynamic calculation. The results showed that the temperature–enthalpy characteristic curve of double-tank sensible TES is well matched with the water-based working medium, which effectively solved the problem of excessive loss caused by the pinch analysis. The exergy efficiency and thermal efficiency were about twice that of the single-stage sensible TES. Based on the above studies, Bian et al. [20] studied the energy level matching of sensible-latent graded TES and adopted a single objective optimization method to optimize the system's exergy efficiency. After optimization, the exergy efficiency of the graded TES increased by 20%.

Due to the internal complexity of the sensible-latent graded TES, the experimental method has some limitations, such as low efficiency, long time consumption, and a large investment. The thermodynamic calculation method can solve this problem. However, thermodynamic calculation of a sensible-latent graded TES is still time-consuming, and the data-driven surrogate models can effectively solve this problem. The artificial neural network (ANN) [21] and support vector machine (SVM) [22] are widely used surrogate models. Compared with the traditional ANNs, the SVM has good generalization ability and can obtain the optimal solution with fewer samples. This method is an intelligent algorithm proposed in 1995 by Cortes and Vapnik. Due to this study's small number of sample points, SVM was chosen to establish the surrogate model.

The sensible-latent graded TES generally considers the two factors of exergy efficiency and cost. While ensuring high exergy efficiency, the cost is also low, resulting in better overall system performance. With the development of computer science, optimization algorithms are more and more widely used in system optimization [23]. Based on the first nondominated sorting genetic algorithm (NSGA), NSGA-II [24] studied the fast nondominated sorting method and crowded comparison operator. Therefore, this algorithm has good global search performance and is the most popular multi-objective optimization algorithm [25]. Rahder et al. [26] applied the NSGA-II method in the optimization of

ice thermal energy storage air conditioning system, and the results showed that energy consumption and annual carbon dioxide emissions were reduced by 11% after optimization. Yuan et al. [27] improved the performance of household air conditioners based on NSGA-II method, saving 20–26% of energy after optimization and about $1.8–3.4 in cost. Li et al. [28] studied the optimization of dish-shaped Brayton system based on NSGA-II method and finally got the optimal solution. However, it was found that there needs to be research on the optimization design of the dish-type graded TES.

In summary, the energy level match for the dish-type sensible-latent graded TES is relatively low. Thus, the system may have low exergy efficiency and high cost. There needs to be more research on the performance optimization design of the dish-type STP. Therefore, this paper intends to study the system's heat storage and release performance by analyzing the effects of different factors on the exergy efficiency of the system. BBD experimental design and response surface methodology were used to analyze the significance of various factors on the cost of graded TES. The prediction model for the exergy efficiency and cost of the sensible-latent graded TES was established using the SVM. The NSGA-II algorithm globally optimizes the graded TES to realize the optimal parameter configuration for the exergy efficiency and cost.

2. System and Method

2.1. System Introduction

Figure 1 illustrates the working process of the dish-type direct steam generation STP system with TES [29–31]. The low-temperature water absorbs the concentrated solar energy in the absorber and turns it into high-temperature and high-pressure steam. Then, the steam drives the turbine to generate electricity and stores/releases energy according to the load. The amount of superheated steam generated by the heat absorber during the daytime operation is far greater than the steam amount required by the system. The excess superheated steam heat is stored in the TES material. When the heat absorber cannot work, it serves as the heat source to supply the system to run normally.
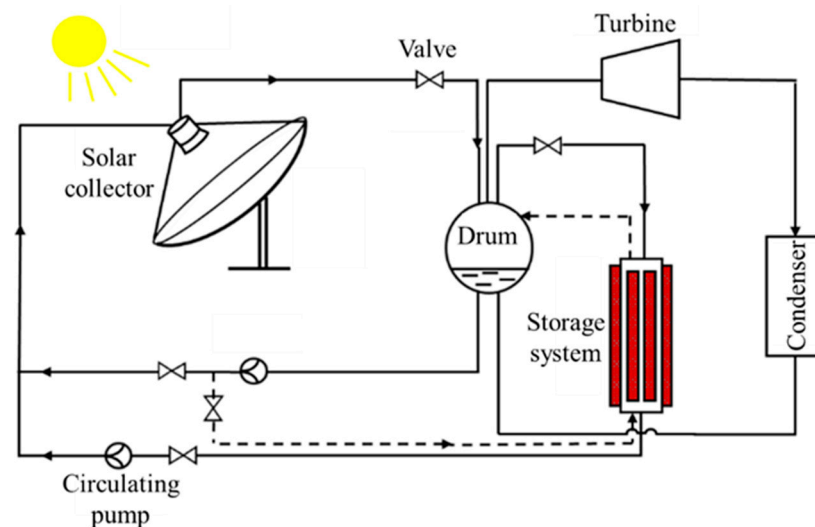
Figure 1. Workflow of the dish-type direct steam thermal power generation system.

Using a two-tank sensible-latent graded TES can effectively solve the difficulty of a single-stage TES by matching the temperature–enthalpy characteristic curve of the working fluid [32–34]. However, the temperature–enthalpy characteristic curve of the working fluid in this system cannot have the same slope for the sensible heat section. The reason is that the specific heat capacity of the superheated steam and liquid water varies greatly. Therefore, an intermediate tank is added between the high-temperature and low-temperature heat exchangers to solve this problem. Figure 2 shows the sensible-latent graded TES sketch map with an intermediate tank.

(A) Charging process

(B) Discharging process
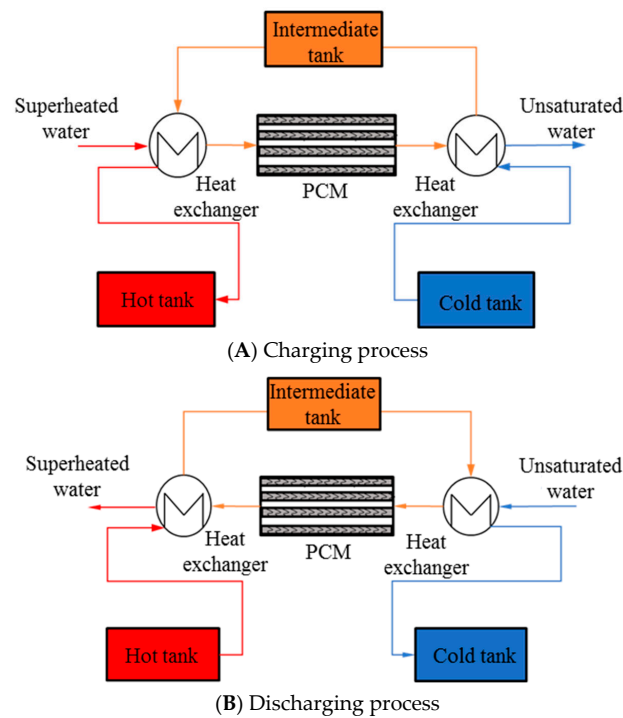
Figure 2. Sensible-latent graded TES with an intermediate tank.

2.2. Theoretical Method of the TES System

The power generation system is a 25 kW dish-type direct steam thermal power generation system. The power generation is in the form of a steam turbine driving a generator to generate electricity. The heat storage time is the operating hours of the steam turbine at night. According to the energy balance, the heat required for normal operation of the turbine during the TES period is called the TES capacity of the TES system. The formula of the heat required for normal operation of the turbo-generator is as follows:

$$Q_0 = \frac{3600 \cdot P_e \cdot t}{\eta_e} \tag{1}$$

where Q_0 is the heat required by the turbo-generator, kJ; P_e is the installed capacity of the power station, kW; t is the TES time, h; and η_e is the absolute electrical efficiency of the turbo-generator.

Heat loss will occur during the operation of the TES system, resulting in insufficient utilization of the stored heat. Therefore, the heat loss of these parts must be considered when calculating the mass of the TES material. The formula for the mass of the TES material in the system is as follows:

$$m = \frac{Q_1}{c_p \cdot \Delta t} = \frac{Q_0}{\eta_2 \cdot c_p \cdot \Delta t} = \frac{3600 \cdot P_e \cdot t}{\eta_e \cdot \eta_2 \cdot c_p \cdot \Delta t} \tag{2}$$

where Q_1 is the total amount of TES, kJ; c_p is the specific heat capacity of the working fluid, kJ/kg·°C; Δt is the TES temperature difference of the TES material, °C; η_2 is the thermal efficiency of the TES system, since the thermal efficiency of the TES system is unknown when calculating the mass of the TES material, it is necessary to perform a certain number of iterations until the equation reaches equilibrium to obtain the total mass of the TES material.

During the process of heat storage and release, the calculation formula for the temperature enthalpy characteristic curve of the system is as follows:

$$Q = m \cdot c_p \cdot \Delta T \tag{3}$$

where Q is the heat change, kJ; m is the mass flow rate of the working fluid, kg/s; c_p is the specific heat capacity of the working fluid, kJ/kg·°C; and ΔT is the temperature difference of the working fluid at different positions, °C.

The exergy analysis method was used to compare and evaluate the thermodynamic performance of the graded TES system [35].

$$Ex = \Delta H - T_e \Delta S \tag{4}$$

where Ex is exergy, kJ; ΔH is the enthalpy change of the working fluid in the TES or heat release process, kJ; T_e is the ambient temperature, °C; and ΔS is the entropy change caused by the heat exchange process, kJ/kg·°C [36,37].

The formula for the entropy change is as follows:

$$\Delta S = m_h c_{p,h} \ln\left(\frac{T_{h,o}}{T_{h,i}}\right) + m_c c_{p,c} \ln\left(\frac{T_{c,o}}{T_{c,i}}\right) \tag{5}$$

where h and c respectively represent the hot- and cold-working fluids, and i and o denote the inlet and outlet.

The exergy efficiency (R_{Ex}) of TES system was obtained by substituting R_{Ex} from Equations (2)–(4) into the following equation.

$$R_{Ex} = \frac{Ex_D}{Ex_C} \tag{6}$$

The effectiveness for high-temperature heat exchangers can be written as [38]:

$$\varepsilon = \frac{1 - \exp\left[-Ntu_H\left(1 - (mc_p)_{\min}/(mc_p)_{\max}\right)\right]}{1 - \left((mc_p)_{\min}/(mc_p)_{\max}\right)\exp\left[-Ntu_H\left(1 - (mc_p)_{\min}/(mc_p)_{\max}\right)\right]} \tag{7}$$

where N_{tuH} is the number of heat transfer units of high-temperature heat exchanger. The outlet temperatures of liquid LBE and superheated steam in high-temperature heat exchanger can be derived from the entry condition and Equation (7).

2.3. Economic Calculation Method for TES System

The cost of the TES system is composed of direct and indirect costs. The direct cost comprises TES material cost, TES tank cost, and miscellaneous cost, and the indirect cost includes tax and engineering cost. Because the research is mainly based on theoretical analysis, only direct costs are considered when calculating the cost of the TES system.

2.3.1. Calculation of TES Tank Parameters

The TES tank is an essential component of the TES system. According to the calculation results of Formula (2), the volume of the TES material is calculated. The calculation formula is as follows:

$$V_1 = \frac{m}{\rho} \tag{8}$$

When calculating the internal volume of the tank, for practical safety considerations, the volume of the TES tank is calculated as 1.15 times the volume of the TES material.

$$V = 1.15 \times V_1 \tag{9}$$

After the calculation result of the Formula (2) is determined, the internal diameter of the tank can be calculated. The calculation method is as follows:

$$d = \sqrt[3]{\frac{4V \cdot n}{\pi}} \tag{10}$$

where n is the ratio of the tank's inner diameter and height. In this paper, this ratio is 3.

2.3.2. Cost Calculation of the TES System

The calculation formula for the cost of TES material is:

$$C_{sm} = C_{sm}^* \cdot M_{sm} \times 10^{-3} \tag{11}$$

where C_{sm} is the cost of TES material; C_{sm}^* is the unit price of the TES material; and M_{sm} is the total mass of the TES material, kg.

The calculation formula for the cost of a single TES tank is:

$$C_{st} = C_{st}^* \cdot \rho_{st} \left(V_{\text{tank}} - 1.15 \frac{M_{sm}}{\rho_{sm}} \right) \times 10^{-3} \tag{12}$$

where C_{st} is the cost of a single TES tank, RMB; C_{st}^* is the unit price of tank steel, yuan/t; ρ_{st} and ρ_{sm} are the density of the steel material and the density of the heat storage material in kg/m^3; V_{tank} is the total volume of the TES tank.

The unit prices of different materials in the calculation of the TES system cost are shown in Table 1.

Table 1. Unit price of different materials in thermal energy storage systems.

Parameter	Numeric (RMB/t)
NaNO$_3$	2548
Solar Salt	3388
Steel tanks	19,403

2.4. Optimization Design Analysis Method

2.4.1. Response Surface Method

When analyzing the significance of factors using the response surface method, the commonly used sample design methods include the central composite design (CCD) and the Box–Behnken design (BBD) [39,40]. Compared with the CCD test, the overall number of test combinations in the BBD test is smaller and thus has higher economic efficiency. Therefore, this paper selects the BBD experimental design for the optimization study and Design Expert 11 was used to design the structural parameter scheme of the graded TES. The BBD method was used to obtain the structural parameter design scheme of the 17-component TES system. The specific structural design parameters are shown in Table 2. The above test scheme was calculated using the thermodynamic and economic calculation program of the graded TES system.

Table 2. Parameter design scheme of Box–Behnken Design.

Number	R_{m}	T_{s} (°C)	m_{s} (kg/s)
1	0.5	650	18
2	0.9	550	22
3	0.5	450	22
4	0.1	450	20
5	0.9	550	18
6	0.5	550	20
7	0.9	650	20
8	0.5	450	18
9	0.5	550	20
10	0.5	650	22
11	0.1	550	18
12	0.5	550	20
13	0.1	650	20
14	0.9	450	20
15	0.1	550	22
16	0.5	550	20
17	0.5	550	20

2.4.2. Data-Driven Surrogate Model

In multi-objective optimization, the physical model has the disadvantages of long computing time and low computing efficiency. Thus, a data-driven surrogate model is established using the SVM [41]. As a fast and efficient forecasting tool, SVM can predict the R_{Ex} and cost of graded TES efficiently and quickly. The surrogate model via the SVM can be expressed as follows:

$$f(x) = \sum_{x_i \in SVM} (\alpha_i - \alpha_i^*) K(x_i - x) + b \tag{13}$$

where α_i, α_i^* is the Lagrange multipliers; b is the undetermined coefficient vector; $K(x_i - x) = \phi(x_i)\phi(x_j)$ is the kernel function.

The surrogate model is implemented using the open-source MATLAB library LIBSVM. LIBSVM provides the linear, polynomial, radial basis (RBF), sigmoid, and precomputed kernel functions. By comparing the adaptability, the present work uses the RBF kernel function. The expression is as follows:

$$K(x_i, x_j) = \exp\left(-\|x_i - x_j\|^2 / 2\gamma^2\right) \tag{14}$$

Figure 3 shows the structure diagram of SVM. Each support vector can be represented by an intermediate node, and the linear combination of the intermediate nodes can obtain the output.
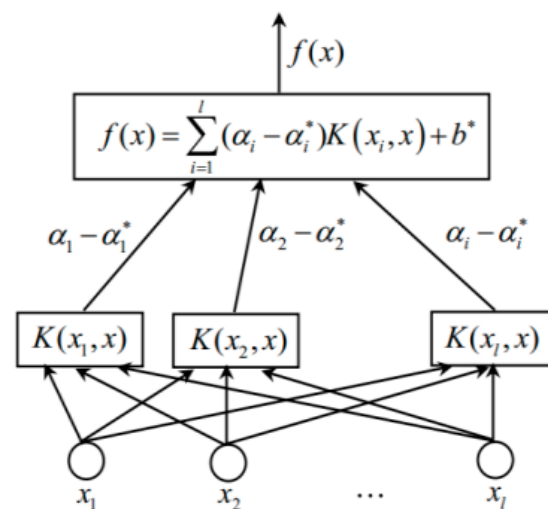
Figure 3. The structure of support vector machine for regression.

Therefore, this study firstly determines the constraint conditions for the optimal design of a graded TES according to the pitch point constraint conditions and uses the BBD experimental design method to obtain the sample solution set required for prediction. Secondly, thermodynamics is applied to calculate the R_{Ex} and total system cost of each design sample to obtain a rapid prediction model of the system.

2.4.3. Multi-Objective Optimization Method

The multi-objective problem usually has multiple objectives, which are mutually exclusive. If one of them increases, the other one decreases. Therefore, multi-objective optimization is not the optimal global solution but a series of optimal solution sets. The goal of multi-objective optimization is to find the Pareto optimal solution set for a specific optimization problem. Figure 4 illustrates the principle of the NSGA-II algorithm. More details about the NSGA-II algorithm are provided elsewhere.
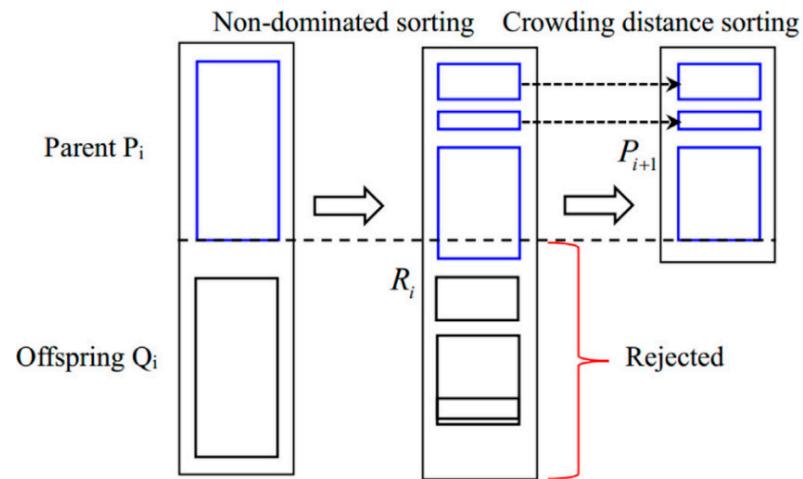
Figure 4. Illustrative representation of the NSGA-II algorithm.

Figure 5 illustrates the optimization flow chart of the NSGA-II algorithm. The fitness functions (i.e., cost parameter and R_{Ex}) are evaluated via SVM using the data-driven surrogate model. The parameter settings are shown in Table 3.
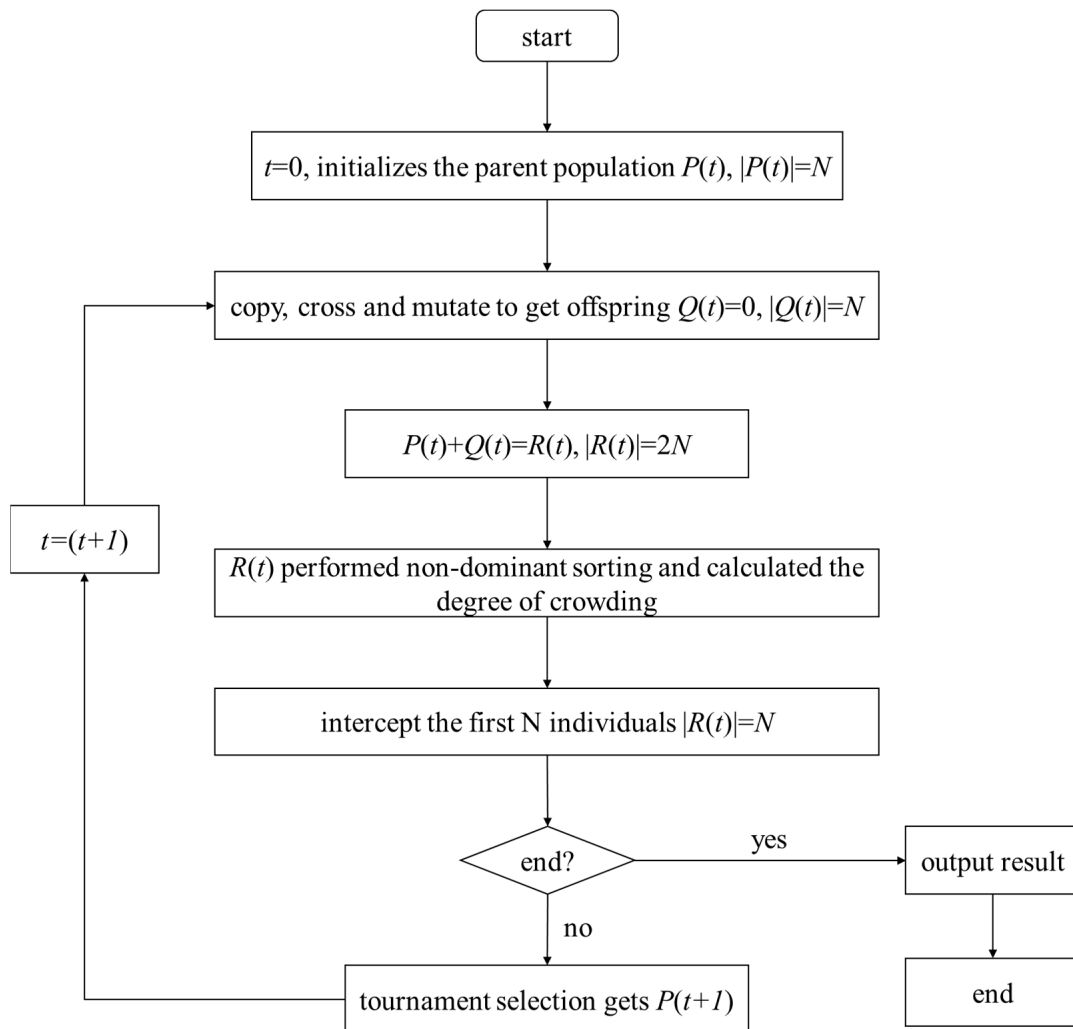
Figure 5. Optimization flow chart of the NSGA-II algorithm.

Table 3. Genetic algorithm parameter settings.

Parameter	Values
Population	200
Probability of crossing: P_c	0.85
Probability of variation: P_m	0.1
Number of iterations	500

3. Results and Discussion

3.1. Analysis of Influencing Factors

In this section, the control variable method is adopted. Different parameters are studied by thermodynamic calculation, including the mass flow rate of the TES material from the cold tank to the intermediate tank (m_s), the superheated steam temperature at the inlet of the system (T_s), and the ratio of the mass flow rate of the regenerative material from the cold tank to the intermediate tank to the thermal material from the intermediate tank to the hot tank (R_m). The calculation case parameters are shown in Table 4.

Table 4. Design table of calculation case.

Number	m_s (kg/s)	T_s (°C)	R_m
Benchmark	20	550	0.5
1	18	550	0.1
2	19	550	0.3
3	20	550	0.5
4	21	550	0.7
5	22	550	0.9
6	20	450	0.5
7	20	500	0.5
8	20	550	0.5
9	20	600	0.5
10	20	650	0.5
11	20	550	0.5
12	20	550	0.5
13	20	550	0.5
14	20	550	0.5
15	20	550	0.5

3.1.1. The Effect of m_s of TES Material on the Graded TES

The T_S and R_m were fixed to study the effect of m_s on the graded TES. The TES conditions with m_s of 18 kg/s, 19 kg/s, 20 kg/s, 21 kg/s, and 22 kg/s were studied. To prevent the sensible TES material from solidifying during the heat storage and release process, the temperature of the sensible TES material in the fixed cold tank is 227 °C. At the same time, the temperature of the working fluid at the outlet was set to 247 °C.

Figure 6 shows the variation in the sensible heat of the superheated steam absorbed by the sensible TES material and the latent TES material with the steam at the system's inlet during the TES process of the graded TES system. It can be seen from the figure that as the m_s of the TES material in the system increases, the sensible heat storage material absorbs heat in the superheated steam section under heat storage condition (Q_{CS}) and the superheated steam section gradually increases, but the latent heat storage material in the superheated steam section absorbs heat under heat storage conditions (Q_{CN}) and gradually decreases. As the m_s of the TES material increases, the temperature of the system hot tank first decreases and then increases. The reason is that when the m_s of the TES material is changed, the heat capacity flow (the product of the m_s and the specific heat capacity) between the TES material and the working fluid changes, which causes the heat exchanger performance to change significantly, which affects the outlet temperature of TES material

of the heat exchanger and the outlet temperature of hot material. Other factors need to be analyzed to obtain the change of the different m_s of the sensible TES material on the TES and release performance of the system.
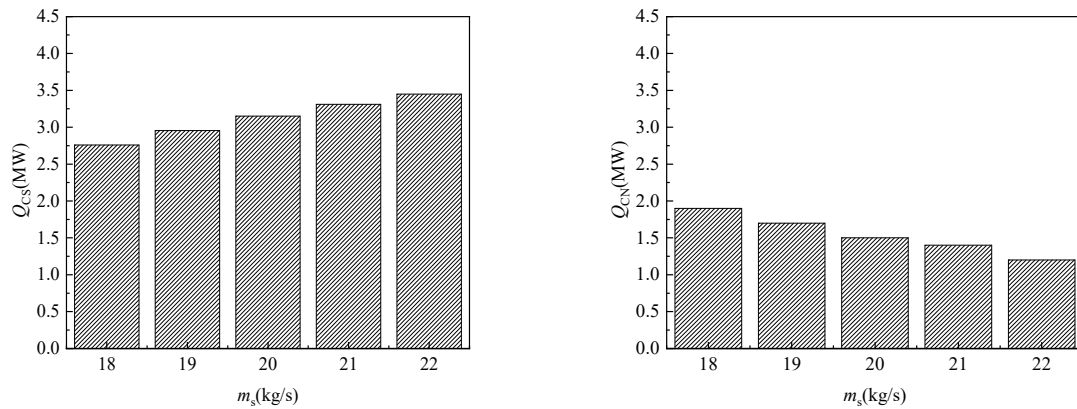
Figure 6. The law of sensible heat absorbed by superheated steam of sensible-latent storage materials increasing with the m_s of TES materials.

Figure 7 shows the variation pattern of the energy level in the high-temperature and low-temperature heat exchangers with the m_s of the TES material during the heat release process. For the energy level heat Q_{DL} in the low-temperature heat exchanger, the m_s of the sensible TES material was increased from 18 kg/s to 22 kg/s, and Q_{DL} increased from 2.4 MW to 2.7 MW. At the same time, the energy level Q_{DH} in the high-temperature heat exchanger rapidly increased from 1.6 MW to 2.0 MW. The figure shows that when the m_s of the working fluid increases from 20 kg/s to 21 kg/s, the energy level heat Q_{DL} of the high-temperature heat exchanger suddenly increases. The primary cause is that the efficiency of the heat exchanger is significantly improved, which increases the heat transfer temperature difference, increasing the energy level of the high-temperature heat exchanger.
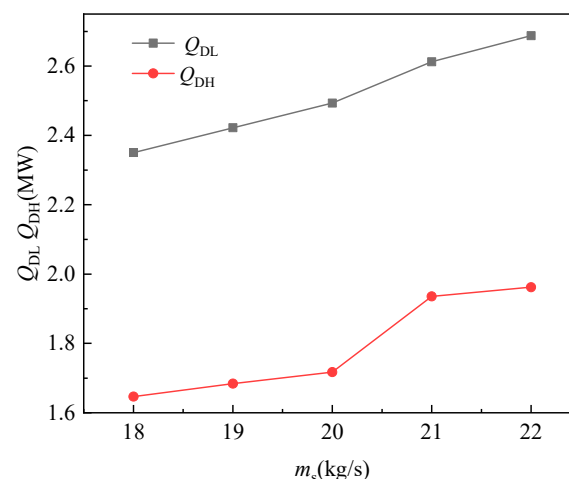
Figure 7. The law of the heat exchange capacity of high and low-temperature heat exchangers increasing with the m_s of TES materials during the heat release process.

Based on the variation pattern of the energy level heat in the high-temperature and low-temperature heat exchangers with the m_s, the storage and release performance of the system is further studied. As shown in Figure 8, when the m_s of the TES material increases, the exergy efficiency of the system R_{Ex} and the thermal efficiency of the system R_Q of the system both decrease. As the m_s of the TES material increased from 18 kg/s to 20 kg/s, the R_{Ex} and R_Q of the system decreased to 87.49% and 86.44%, respectively. As the m_s of

the TES material increases from 20 kg/s to 21 kg/s, the change in efficiency reduces the energy level of the low-temperature heat exchanger during the process of heat release. It simultaneously increases the energy level of the high-temperature heat exchanger, which eventually leads to the R_{Ex} of the system's significant increase.
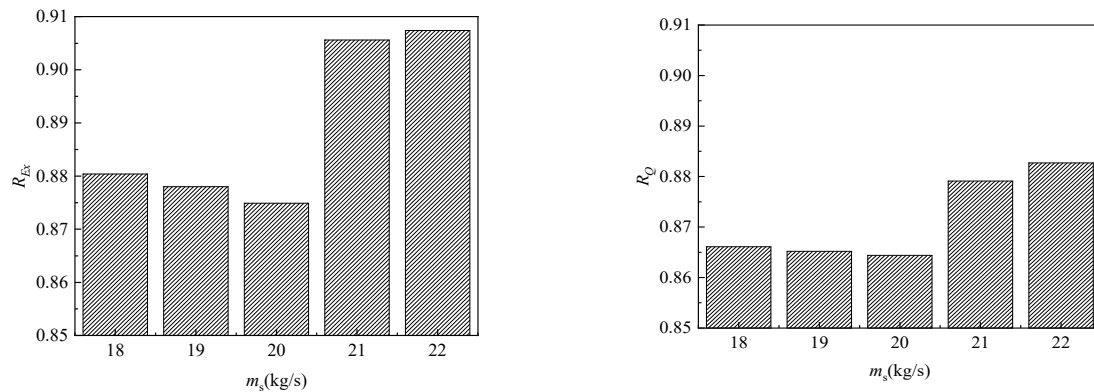
Figure 8. The law of the heat exchange capacity of high- and low-temperature heat exchangers increases with the m_s of TES materials during the process of heat release.

3.1.2. Effect of T_S on the Graded TES System

When studying the effect of system inlet steam on the graded TES system, the fixed variable method was also used to study the working conditions of the T_S of 450 °C, 500 °C, 550 °C, 600 °C, and 650 °C.

Figure 9 shows the curve of sensible heat absorbed by superheated steam in the heat storage process in the graded TES. It can be seen from the figure that as the temperature of the superheated steam at the inlet of the system increases, the Q_{CS} and Q_{CN} of the superheated steam section gradually increase. Moreover, with the increase in superheated steam temperature, the growth rate of Q_{CS} is greater than the growth rate of Q_{CN}. Since the amount of heat used to absorb the latent heat of the working fluid in the latent TES energy level remains unchanged, it can be concluded that when the temperature of the superheated steam at the inlet of the system is changed, the heat increase of the energy level of the high-temperature heat exchanger is much larger than that of the phase change TES energy level, considering that the energy level matching of TES materials under TES conditions is not sufficient to explain the effect of energy level matching on the overall TES and release performance of the graded TES system. Therefore, it is necessary to study the energy level matching in the exothermic process systematically.
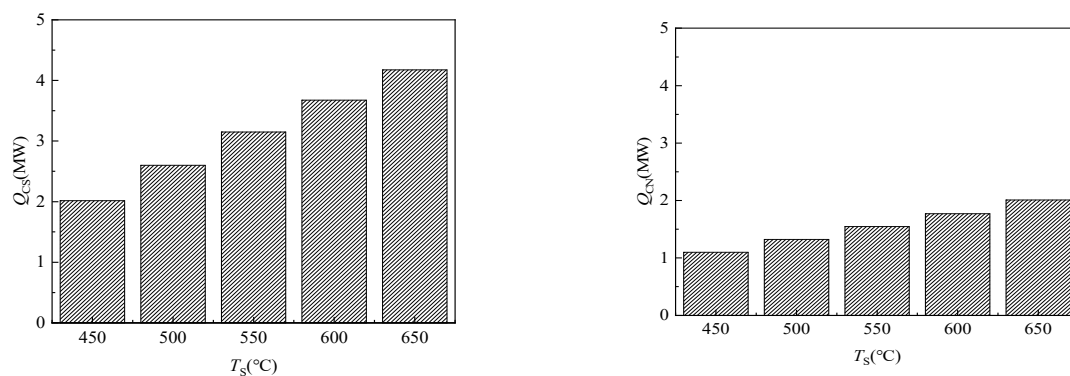
Figure 9. The law of sensible heat absorbed by sensible-latent storage materials increasing with the inlet steam temperature of the system.

Figure 10 shows the variation pattern of the energy level of the high- and low-temperature heat exchangers with the T_S during the heat release process. For the energy

level heat Q_{DL} of the low-temperature heat exchanger, as the T_S increases from 450 °C to 650 °C, Q_{DL} gently increases from 2.1 MW to 2.3 MW. Meanwhile, the high-temperature heat exchanger heat exchange Q_{DH} rapidly increased from 1.2 MW to 2.3 MW. From the above data, it can be seen that during the heat release process, the energy level heat of the high- and low-temperature heat exchangers gradually increases with increasing T_S; the energy level heat and heat loss of the low-temperature heat exchanger increase slightly with increasing T_S. The high-temperature heat exchanger's energy level heat and heat loss increased significantly with increasing TS, and the change was dramatic. From the numerical analysis of the energy level heat, the energy level heat of the low-temperature heat exchanger always has a relatively large impact on the TES and release performance of the graded TES system, but the resulting system exergy loss does not significantly increase with the increase in the inlet superheated steam. On the other hand, as the temperature of the superheated steam at the inlet of the system increases, the energy level of the high-temperature heat exchanger increases significantly, and the corresponding exergy loss increases significantly. Therefore, for the exothermic process, the increase in the exergy loss caused by the increase in the T_S is principal because of the change in the energy level of the high-temperature heat exchanger.
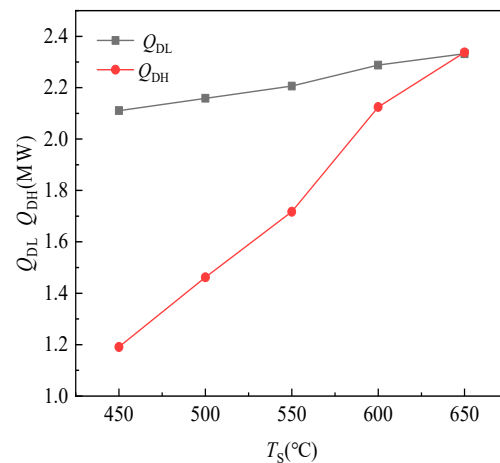
Figure 10. The law of the heat exchange rate of high and low-temperature heat exchangers rising with the inlet steam temperature of the system during heat release.

The variation pattern of the R_{Ex} and R_Q of the system with the T_S is shown in Figure 11. As the inlet superheated steam increases, the R_{Ex} and R_Q of the system both decrease. As the T_S increased from 450 °C to 650 °C, the R_{Ex} of the system decreased from 92.9% to 85.5%. The R_Q also showed a decreasing trend with the decrease in the superheated steam inlet temperature, and the R_Q of the system decreased from 92.19% to 83.06%.
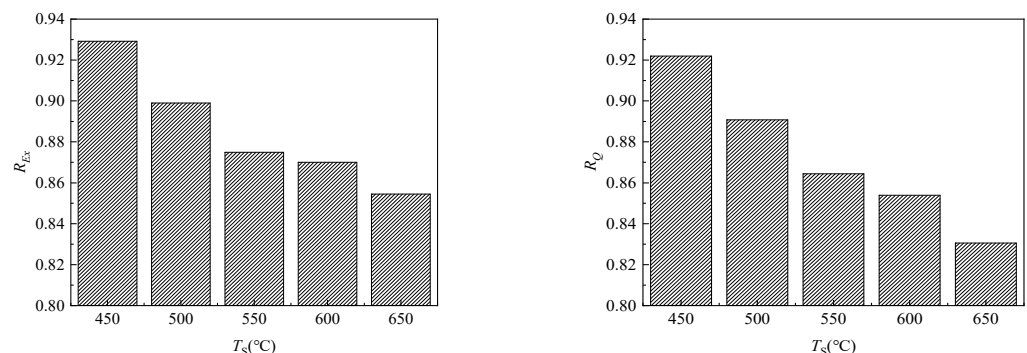
Figure 11. The law of R_{Ex} and t R_Q increasing with T_S.

3.1.3. Effect of the TES Material R_m on the Graded TES System

When studying the effect of the TES material R_m, the fixed variable method was also used to study the TES system working conditions when the TES material R_m is 0.1, 0.3, 0.5, 0.7, and 0.9. Based on the temperature–enthalpy characteristic curve, the Rm's effect on the graded TES's energy level matching was analyzed.

Figure 12 shows the variation in the sensible heat of the superheated steam absorbed by the sensible TES material with the R_m. It can be seen from the figure that as the R_m of the TES material increases, the Q_{CS} of the superheated steam section gradually increases, but the Q_{CN} gradually decreases. Due to the control of factors such as the T_S, the outlet temperature of the TES material gradually decreases. Other factors need to be analyzed to obtain the change of the different Rm of the sensible TES material more clearly on the TES and release performance of the system.
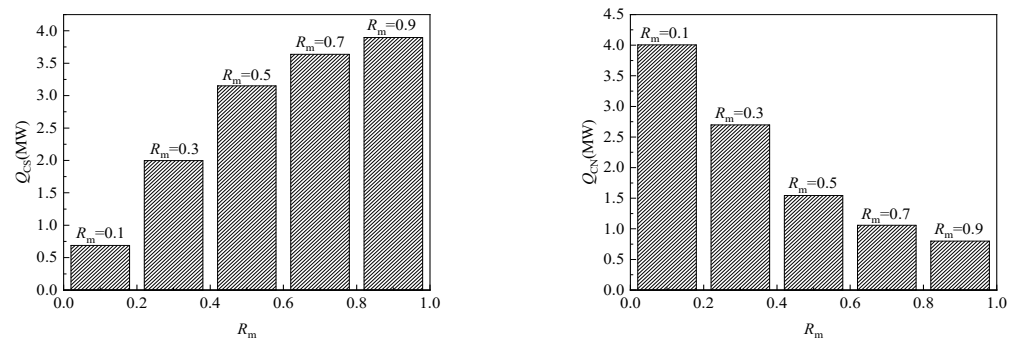
Figure 12. The law of sensible heat absorbed by superheated steam of sensible-latent storage materials increases with the R_m of TES materials.

The variation pattern of the R_{Ex} and R_Q of the system with the R_m of the TES material is shown in Figure 13. As the R_m of the TES material increases, the R_{Ex} and R_Q of the system both increase. As the R_m of the TES material increases from 0.1 to 0.9, the R_{Ex} and R_Q of the system increase from 78.50% to 92.91%. Meanwhile, the R_Q increased with the R_m of the TES material, from 77.47% to 91.08%.
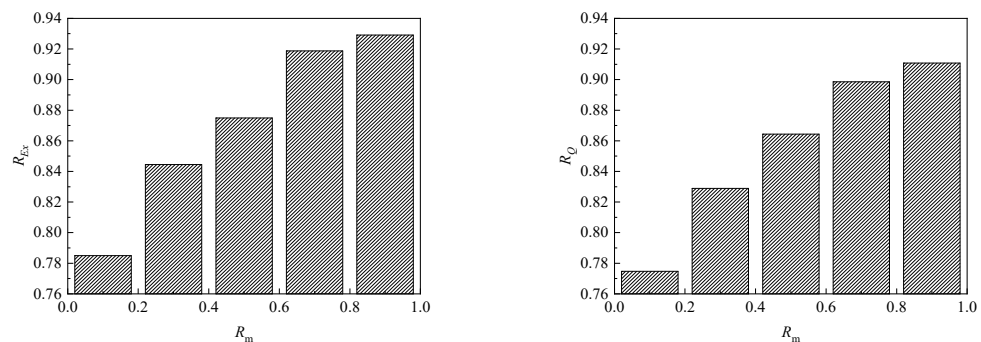
Figure 13. The law of system R_{Ex} and R_Q increasing with the R_m of TES materials in the heat release process.

3.2. Response Surface Method

Figure 14 shows the comparison between the actual calculated value and the predicted value using the graded TES system cost model as the optimization target. According to the distribution of the calculation results of different design combinations in the figure, the actual values are basically distributed near the prediction line of the regression model, indicating that the calculated results are basically consistent with the predicted values, and the prediction results of the regression model have high accuracy.
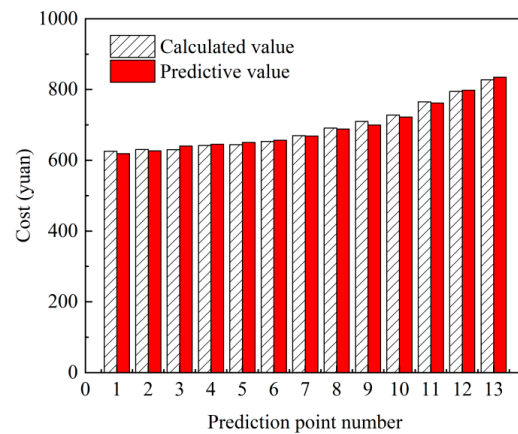
Figure 14. Analysis chart of the calculated cost value and test predicted value.

To further discuss the impact of each variable of the two-tank sensible-latent graded TES system on the system cost, Figure 15 shows the cost changes of the graded TES system under different system parameters. Figure 15a shows the interaction response surface diagram of the system cost between the superheated steam temperature and the sensible TES material mass flow at the inlet and outlet of the graded TES system when the R_m of the sensible TES material at the inlet and outlet of the graded TES system is 0.5. It can be seen from the figure that as the inlet steam temperature of the system increases, the system cost changes significantly. Taking the TES material m_s of 18 kg/s as an example, when the system steam inlet temperature increases from 450 °C to 650 °C, the system cost increases from RMB 6.41 m to RMB 6.87 m. In comparison, when the steam inlet temperature of the system is 450 °C, the system cost only rises from RMB 6.41 m to RMB 6.56 m when the m_s of the TES material changed.

(a)

(b)

Figure 15. *Cont.*

(c)
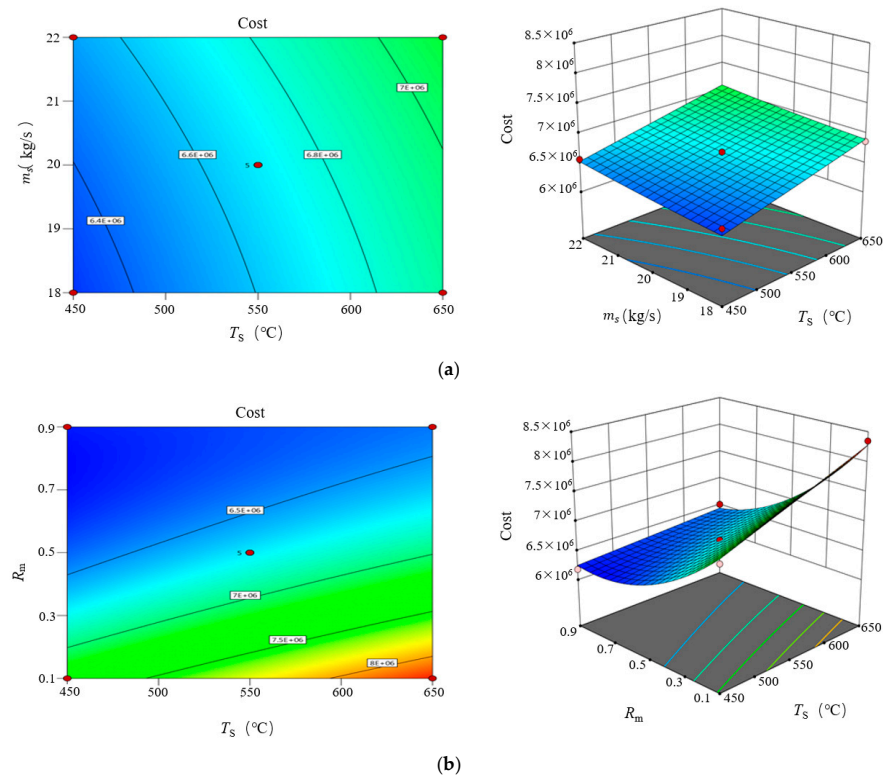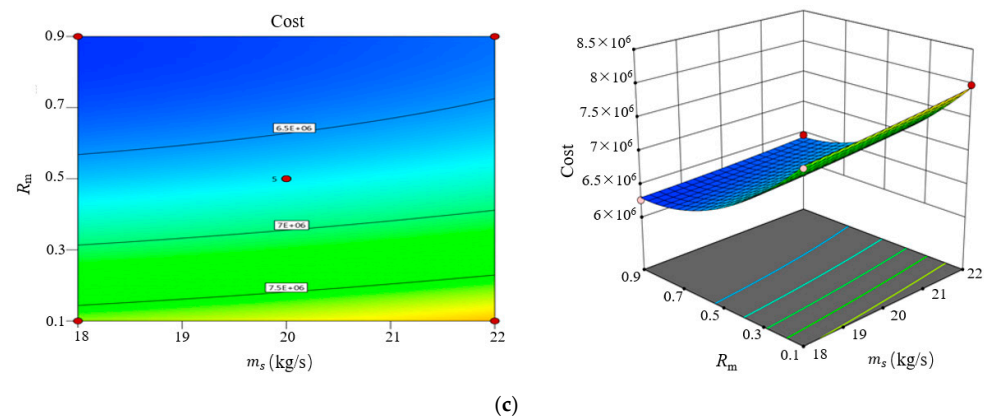
Figure 15. Interaction of different design variables on the cost of graded multistage TES system. (**a**) Response surface diagram of the interaction between superheated steam temperature and m_s of TES material on system cost. (**b**) Response surface diagram of the interaction between superheated steam temperature and R_m of TES materials for system cost. (**c**) Response surface diagram of the interaction between m_s of TES material and R_m of TES material to system cost.

Figure 15b shows the response surface diagram of the interaction between the superheated steam temperature at the inlet of the system and the R_m of sensible TES material on the system cost when the m_s of the sensible TES material in the graded TES system is 20 kg/s. The figure shows that the R_m of the TES material and the temperature of the superheated steam at the inlet of the system have a large impact on the system cost, and the system cost changes significantly with the change in parameters. Taking the TES material R_m as an example, when the system steam inlet temperature increased from 450 °C to 650 °C, the system cost increased from RMB 7.21 m to RMB 8.35 m; when the system steam inlet temperature was 450 °C, the R_m of the TES material is changed, the system cost was only reduced from RMB 7.21 m to RMB 6.18 m.

Figure 15c shows the interaction response surface of the sensible TES material R_m and the sensible TES material m_s on the system cost when the inlet steam temperature of the graded TES system is 550 °C. It can be seen from the figure that as the R_m of the system sensible TES material increases, the system cost changes significantly. Taking the m_s of the TES material as 18 kg/s as an example, when the m_s of the sensible TES material in the system increases from 0.1 to 0.9, the system cost is reduced from RMB 7.62 m to RMB 6.26 m. In comparison, when the R_m of the TES material in the system is 0.1, the system cost only rises from RMB 7.62 m to RMB 7.99 m when the m_s of the TES material is changed.

3.3. Rapid System Prediction Model Based on Support Vector Machine

The thermodynamic calculation results of the above BBD design samples were used to establish a fast model of the graded TES, the R_{Ex} and cost of the system were determined. The comparison results are shown in Figure 16. The results of the comparison between the predicted values and the calculated values of most of the design samples are good, which proves the reliability of the prediction model. Through the analysis, the prediction results of the SVM were compared with the thermodynamic calculation. The maximum errors were 4.39% and 3.26%, and mean deviation value was 0.86% and 0.82%. In summary, the SVM rapid prediction model obtained in this work has high accuracy and can accurately and rapidly predict the R_{Ex} and cost of the graded TES.

3.4. Multi-Objective Optimization Based on the NSGA-II Algorithm

The multi-objective optimization of the graded TES system studied in this section uses the R_m of the TES material at the inlet and outlet of the system buffer tank, the T_S, and the R_m of the TES material as the optimized fitness values. The overall cost is used as two functions of the optimization objective. Figure 17 shows the calculation results.
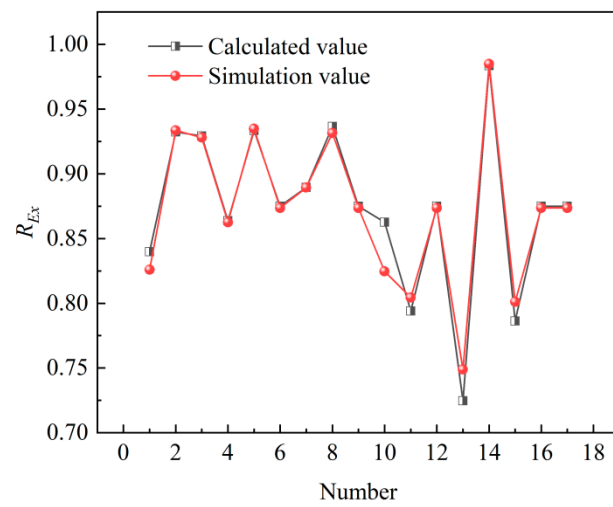
(**a**) exergy efficiency
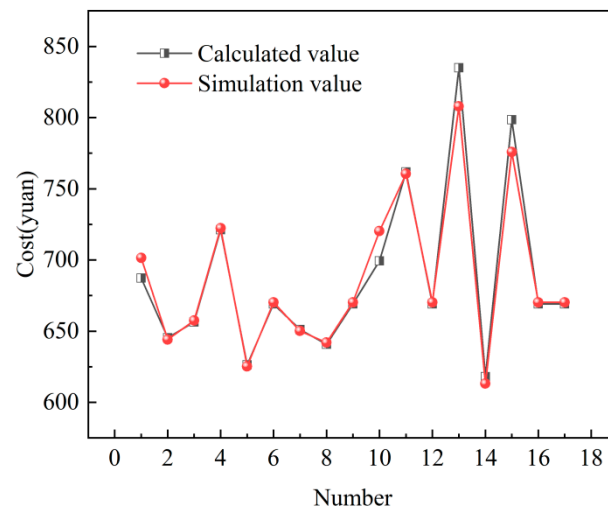
(**b**) cost

Figure 16. Comparison between the support vector machine's predicted value and calculated value.
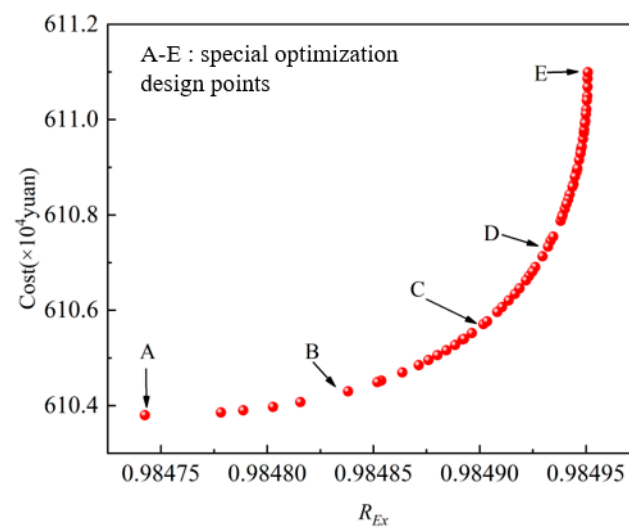
Figure 17. Pareto optimal solutions for the graded multistage TES system.

It can be analyzed from the optimization implementation results in the figure that a total of 60 nondominant Pareto optimal solution sets are obtained. The variance trend of the two targets in the figure is not obvious. The primary cause is that when the R_m of the system sensible TES material and the inlet super steamed steam temperature reaches the optimal value, the R_{Ex} and cost of the system have been basically determined and will only fluctuate slightly with the variation of m_s of TES materials. This also confirms that the factors in the response surface method affect the research results. There are five special optimization design points in the optimization solution set. The R_{Ex} and cost at point A are at the lowest level, and the R_{Ex} and cost at point E are at the highest level. In the process of moving from point A to point B, the R_{Ex} increase is more significant than cost increases, and while moving from point D to point E, the significance of the increase in cost is much greater than the significance of the increase in R_{Ex}. In the two-tank sensible-latent graded TES system studied in this paper, point C is an optimal design point for the R_{Ex} and cost of the system. Table 5 shows the corresponding factor design.

Table 5. Optimal design results of multi-objective optimization on point C for the graded TES system.

Design Variables	Optimization Results
R_m	0.9
T_S	450 °C
m_s	19.1 kg/s

Figure 18 compares the calculation results of R_{Ex} and cost at point C and the results of multi-objective optimization. As shown in the figure, according to the comparison, it was found that the difference between the calculation results of R_{Ex} and cost and the multi-objective optimization result is 0.0001 and RMB 36,000, respectively, and the error is within the allowable range. In addition, the R_{Ex} and cost of the graded TES can be accurately predicted by the prediction model.
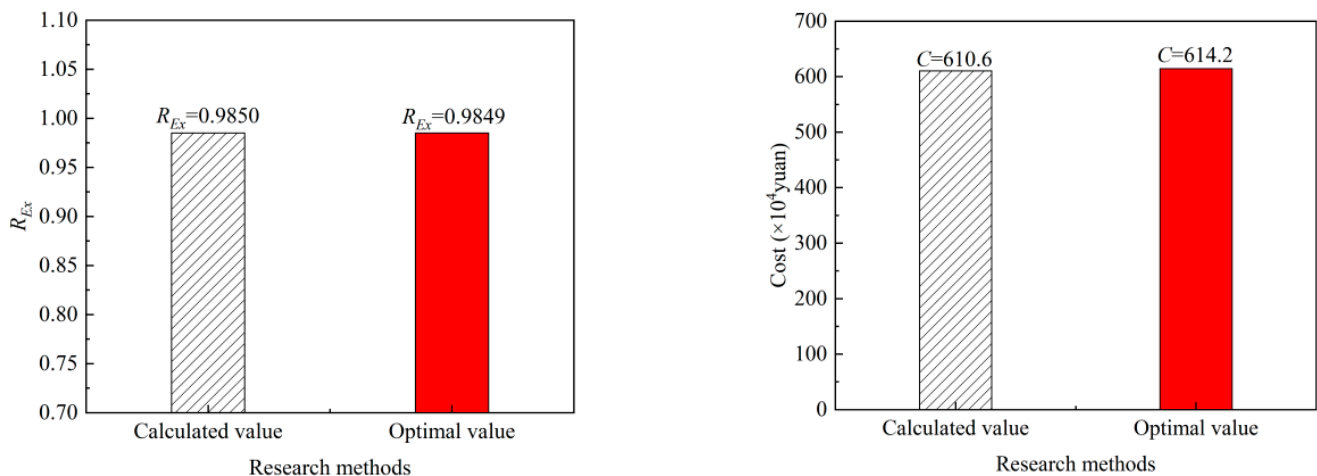
Figure 18. Multi-objective optimization simulation verification diagram of the graded TES system.

Figure 19 compares the calculation results of the R_{Ex} and cost of the samples before and after optimization. As shown in the figure, the results show that after optimization, the calculation result of R_{Ex} is 11.01% higher than that before optimization, and the cost calculation result after optimization is reduced by RMB 585,000 compared with that before optimization. It proves that the optimization model has a significant optimization effect while ensuring high accuracy.
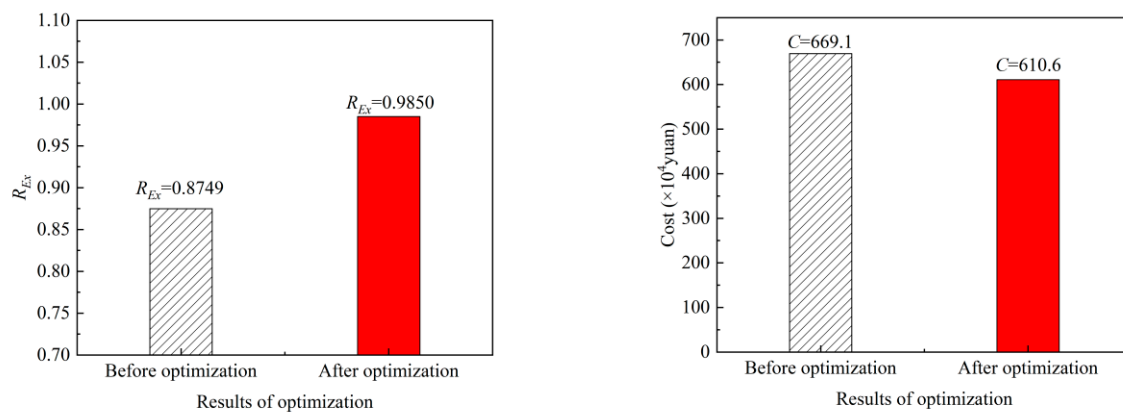
Figure 19. Comparison of the graded TES system before and after optimization.

4. Conclusions

The present study established a data-driven surrogate model for a two-tank sensible-latent graded TES system by using the SVM. Then, the NSGA-II algorithm is used for multi-objective optimization of the graded TES system, in which the efficiency and cost of the graded TES are calculated using the surrogate model. The conclusions of the study are as follows:

1. Using the response surface method as the objective function, the significance of the impact of the three factors is studied. The results show that the system T_S and the R_m of the sensible TES material have a significant impact on the system cost, and there is an optimal mass flow of sensible TES material, thereby maximizing the overall performance of the system.
2. The rapid cost prediction model of the graded TES based on SVM is trained. The results showed that the predicted cost was in good agreement with the thermodynamic calculation results. The maximum error is 3.26%, and the average error is 0.82%, which aligns with the demand for rapid performance prediction of the graded TES system.
3. By comparing the R_{Ex} and cost corresponding to design point C obtained from the multi-objective optimization with the thermodynamic calculation results, the R_{Ex} calculation result after optimization was 11.01% higher than that before optimization, and the cost calculation result after optimization was 585,000 yuan less than that before optimization. Its accuracy is at a high level, and the optimization effect is obvious.

Author Contributions: Conceptualization, B.Y.; Methodology, Z.Z. and R.B.; Investigation, Z.Z.; Writing—original draft, Z.Z.; Writing—review & editing, Y.D. and D.S.; Visualization, Z.Z.; Funding acquisition, Y.D. and B.Y. All authors have read and agreed to the published version of the manuscript.

Data Availability Statement: Not applicable.

Abbreviations

Q	heat quantity (kJ)
p	working pressure (MPa)
t	time (h)
η	efficiency (%)
Ex	exergy(W)
c_p	specific heat (J/kg·K)

T	temperature (°C)
H	enthalpy (J)
S	entropy (J/K)
V	volume (m^3)
n	ratio of the tank's inner diameter and height (-)
C	cost (RMB)
ρ	density

Greek letters

ε	efficiency of heat exchanger[-]
Δ	difference[-]

Subscripts

0	turbo-generator
e	environment
c	cold
h	hot
sm	Thermal energy storage material
st	steel material
*	unit price
TES	Thermal energy storage
STP	solar thermal power
ANN	artificial neural network
SVM	support vector machine
NSGA	nondominated sorting genetic algorithm
CCD	central composite design
BBD	Box–Behnken design

References

1. Al-Habaibeh, A.; Shakmak, B.; Fanshawe, S. Assessment of a novel technology for a stratified hot water energy storage—The water snake. *Appl. Energy* **2018**, *222*, 189–198. [CrossRef]
2. Guo, S.; Liu, Q.; Sun, J.; Jin, H. A review on the utilization of hybrid renewable energy. *Renew. Sustain. Energy Rev.* **2018**, *91*, 1121–1147. [CrossRef]
3. Liu, L.; Wang, R.; Wang, Y.; Li, W.; Sun, J.; Guo, Y.; Qu, W.; Li, W.; Zhao, C. Comprehensive analysis and optimization of combined cooling heating and power system integrated with solar thermal energy and thermal energy storage. *Energy Convers. Manag.* **2023**, *275*, 116464. [CrossRef]
4. Ravi Kumar, K.; Krishna Chatanya, N.V.V.; Sendhil Kumar, N. Solar thermal energy technologies and its applications for process heating and power generation—A review. *J. Clean. Prod.* **2021**, *282*, 125296. [CrossRef]
5. Zayed, M.E.; Zhao, J.; Li, W.; Sadek, S.; Elsheikh, A.H. Applications of Artificial Neural Networks in Concentrating Solar Power Systems. In *Artificial Neural Networks for Renewable Energy Systems and Manufacturing Applications*; Academic Press: Cambridge, MA, USA, 2021.
6. Behar, O. Solar thermal power plants—A review of configurations and performance comparison. *Renew. Sustain. Energy Rev.* **2018**, *92*, 608–627. [CrossRef]
7. Zayed, M.E.; Zhao, J.; Elsheikh, A.H.; Li, W.; Sadek, S.; Aboelmaaref, M.M. A comprehensive review on Dish/Stirling concentrated solar power systems: Design, optical and geometrical analyses, thermal performance assessment, and applications. *J. Clean. Prod.* **2021**, *283*, 124664. [CrossRef]
8. Milian, Y.E.; Ushak, S.; Cabeza, L.F.; Grageda, M. Advances in the development of latent heat storage materials based on inorganic lithium salts. *Sol. Energy Mater. Sol. Cells* **2020**, *208*, 110344. [CrossRef]
9. Suresh, C.; Saini, R.P. Thermal performance of sensible and latent heat thermal energy storage systems. *Int. J. Energy Res.* **2020**, *44*, 4743–4758. [CrossRef]
10. Ben Khedher, N.; Bantan, R.A.; Kolsi, L.; Omri, M. Performance investigation of a vertically configured LHTES via the combination of nano-enhanced PCM and fins: Experimental and numerical approaches. *Int. Commun. Heat Mass Transf.* **2022**, *137*, 106246. [CrossRef]
11. Ben Khedher, N.; Ben Nasrallah, S. Three-Dimensional Simulation of a porous thermal energy storage system using solid-liquid phase change material. *J. Porous Media* **2011**, *14*, 777–790.
12. Wang, K.; Jia, P.-S.; Zhang, Y.; Zhang, Z.-D.; Wang, T.; Min, C.-H. Thermal-fluid-mechanical analysis of tubular solar receiver panels using supercritical CO_2 as heat transfer fluid under non-uniform solar flux distribution. *Sol. Energy* **2021**, *223*, 72–86. [CrossRef]

13. Malviya, R.; Agrawal, A.; Baredar, P.V. A comprehensive review of different heat transfer working fluids for solar thermal parabolic trough concentrator. *Mater. Today Proc.* **2021**, *46*, 5490–5500. [CrossRef]
14. Yilmazoglu, M.Z. Effects of the selection of heat transfer fluid and condenser type on the performance of a solar thermal power plant with technoeconomic approach. *Energy Convers. Manag.* **2016**, *111*, 271–278. [CrossRef]
15. Laing, D.; Bahl, C.; Bauer, T.; Lehmann, D.; Steinmann, W.-D. Thermal energy storage for direct steam generation. *Sol. Energy* **2011**, *85*, 627–633. [CrossRef]
16. Eck, M.; Eickhoff, M.; Fontela, P.; Gathmann, N.; Meyer-Grünefeldt, M.; Hillebrand, S.J.; Schulte-Fischedick, J. Direct Steam Generation in parabolic troughs at 500 °C—First results of the REAL-DISS project. In Proceedings of the 17th Solar PACES Conference, Granada, Spain, 20–23 September 2011.
17. Seitz, M.; Cetin, P.; Eck, M. Thermal storage concept for solar thermal power plants with direct steam generation. *Energy Procedia* **2014**, *49*, 993–1002. [CrossRef]
18. Eck, M.; Eickhoff, M.; Fontela, P.; Laing, D.; Meyer-Grünefeldt, M.; Möllenhoff, M.; Nölke, M.; Vives, F.O.; Riffelmann, K.-J.; Sanchez-Biezma, A.; et al. Test and demonstration of the direct steam generation (DSG) at 500 °C. In Proceedings of the Solar PACES 2009—Electricity, Fuels and Clean Water Powered by the Sun, Berlin, Germany, 15–18 September 2009.
19. Chen, Q.; Liang, X.-G.; Guo, Z.-Y. Entransy theory for the optimization of heat transfer—A review and update. *Int. J. Heat Mass Transf.* **2013**, *63*, 65–81. [CrossRef]
20. Bian, R.; Deng, Y.; Feng, C. Performance and optimization study of graded thermal storage system for direct steam generation dish type solar thermal power. 2022; *under review.*
21. Gumar, A.K.; Demir, F. Solar photovoltaic power estimation using meta-optimized neural networks. *Energies* **2022**, *15*, 8669. [CrossRef]
22. Cortes, C.; Vapnik, V. Support-Vector Networks. *Mach. Learn.* **1995**, *20*, 273–297. [CrossRef]
23. Zhang, J.; Zhu, H.; Yang, C.; Li, Y.; Wei, H. Multi-objective shape optimization of helico-axial multiphase pump impeller based on NSGA-II and ANN. *Energy Convers. Manag.* **2011**, *52*, 538–546. [CrossRef]
24. Verma, S.; Pant, M.; Snasel, V. A Comprehensive Review on NSGA-II for Multi-Objective Combinatorial Optimization Problems. *IEEE Access* **2021**, *9*, 57757–57791. [CrossRef]
25. Deb, K.; Pratap, A.; Agarwal, S.; Meyarivan, T.A.M.T. A fast and elitist multiobjective genetic algorithm: NSGA-II. *IEEE Trans. Evol. Comput.* **2002**, *6*, 182–197. [CrossRef]
26. Hoseini Rahdar, M.; Heidari, M.; Ataei, A.; Choi, J.-K. Modeling and optimization of R-717 and R-134a ice thermal energy storage air conditioning systems using NSGA-II and MOPSO algorithms. *Appl. Therm. Eng.* **2016**, *96*, 217–227. [CrossRef]
27. Yuan, X.; Cheng, W. Multi-objective optimization of household refrigerator with novel heat-storage condensers by Genetic algorithm. *Energy Convers. Manag.* **2014**, *84*, 550–561. [CrossRef]
28. Li, Y.; Liu, G.; Liu, X.; Liao, S. Thermodynamic multi-objective optimization of a solar-dish Brayton system based on maximum power output, thermal efficiency and ecological performance. *Renew. Energy* **2016**, *95*, 465–473. [CrossRef]
29. Gao, D.; Li, J.; Ren, X.; Hu, T.; Pei, G. A novel direct steam generation system based on the high-vacuum insulated flat plate solar collector. *Renew. Energy* **2022**, *197*, 966–977. [CrossRef]
30. Hirsch, T.; Eck, M. Design of a phase separation system for a direct steam generation parabolic trough collector field. *J. Sol. Energy Eng. -Trans. Asme* **2008**, *130*, 011003. [CrossRef]
31. Zarza, E.; Valenzuela, L.; León, J.; Hennecke, K.; Eck, M.; Weyers, H.-D.; Eickhoff, M. Direct steam generation in parabolic troughs: Final results and conclusions of the DISS project. *Energy* **2004**, *29*, 635–644. [CrossRef]
32. Li, X.; Xu, E.; Song, S.; Wang, X.; Yuan, G. Dynamic simulation of two-tank indirect thermal energy storage system with molten salt. *Renew. Energy* **2017**, *113*, 1311–1319. [CrossRef]
33. Peiró, G.; Prieto, C.; Gasia, J.; Jové, A.; Miró, L.; Cabeza, L.F. Two-tank molten salts thermal energy storage system for solar power plants at pilot plant scale: Lessons learnt and recommendations for its design, start-up and operation. *Renew. Energy* **2018**, *121*, 236–248. [CrossRef]
34. Wan, Z.; Wei, J.; Qaisrani, M.A.; Fang, J.; Tu, N. Evaluation on thermal and mechanical performance of the hot tank in the two-tank molten salt heat storage system. *Appl. Therm. Eng.* **2020**, *167*, 114775. [CrossRef]
35. Bejan, A. Entropy Generation Minimization. In *Advanced Engineering Thermodynamics*; John Wiley & Sons: New York, NY, USA, 1995.
36. Guo, J.; Huai, X.; Cheng, K. The comparative analysis on thermal storage systems for solar power with direct steam generation. *Renew. Energy* **2018**, *115*, 217–225. [CrossRef]
37. Guo, J.; Huai, X. Optimization design of heat exchanger in an irreversible regenerative Brayton cycle system. *Appl. Therm. Eng.* **2013**, *58*, 77–84. [CrossRef]
38. Shah, R.K.; Sekulic, D.P. Fundamentals of heat exchanger design. In *Fundamentals of Heat Exchanger Design*; John Wiley & Sons: New York, NY, USA, 2002.
39. Yusri, I.M.; Abdul Majeed, A.P.P.; Mamat, R.; Ghazali, M.F.; Awad, O.I.; Azmi, W.H. A review on the application of response surface method and artificial neural network in engine performance and exhaust emissions characteristics in alternative fuel. *Renew. Sustain. Energy Rev.* **2018**, *90*, 665–686. [CrossRef]

40. Mohammadi, M.M.; Vossoughi, M.; Feilizadeh, M.; Rashtchian, D.; Moradi, S.; Alemzadeh, I. Effects of electrophoretic deposition parameters on the photocatalytic activity of TiO$_2$ films: Optimization by response surface methodology. *Colloids Surf. A Physicochem. Eng. Asp.* **2014**, *452*, 1–8. [CrossRef]

41. Shan, Z.; Luo, H.; Qin, S.H. Polymer ratio optimization based on support vector machine and genetic algorithm. *Appl. Mech. Mater.* **2013**, *444–445*, 1026–1032. [CrossRef]